# Exploration of the Internal Energy Effect on 3D-Casson Fluid Embedded by Porous Media over A Rotating Sheet

Alfunsa Prathiba, A. Venkata Lakshimi

***Abstract* — Viscous dissipation acts as an energy source and alters the temperature distribution, and extremely shear flows impact the fluid flow structure. Thus, the current study analyses the three-dimensional rotating Casson fluid flow across a linear extending sheet in the existence of internal energy and porous medium. The controlling equations for velocity, concentration, and energy of the steady flow are provided and simplified using the similarity transformations. The three-staged collocation technique, namely Lobatto III A was implemented in conjunction with MATLAB to solve the resulting equations. The physical characteristics of the relevant quantities were explained with the support of graphs. It was noticed that the velocity component decreased with the rise in the porosity parameter. For the improved values of the Eckert number, the temperature component increased. The influence of Eckert number, Casson parameter etc. on the Skin friction, the Nusselt number and the Sherwood number were assessed.**

***Keywords* — Eckert number, Lobatto III A collocation method, Porosity, Rotating fluid, Viscous Dissipation, 3-D Casson fluid.**

## I. Introduction

The investigation of rotational fluid flow, which originates from the "Coriolis force", has important uses in geophysical situations, astrophysics, oceanography, and other fields. Moreover, this type of flow across a stretched surface is used in a variety of industries, including yarn spinning, plastic sheet extrusion, food processing, and glass wafting [1]. Rotating flows are additionally used in geotechnical manufacturing, such as centrifugal purification, turbines, material treating, and rotatory hydromagnetic generators [2].Reference [3] investigated the rotating fluid flow problem using a two-dimensional stretchable surface. Furthermore, when the rotation parameter´ was larger than unity´, Wang acquired a more precise solution employing the analytic approach than the numerical approach. Several scholars looked into the peculiarities of flow behaviour when rotation was taken into account[2], [4]–[12], [13].

Fluids are a need for existence, and scientists have uncovered many statistics and illustrations about fluid movement due to their importance in natural and industrial processes. Fluid dynamics is the study of fluid flow and how forces affect it. It demonstrates how to explain star evolution, weather phenomena, sea currents, and blood circulation using an approach. "Archimedes was a Greek mathematician" who studied the buoyancy and statics of fluids before formulating the Archimedes principle, which is considered the earliest contribution to fluid mechanics. In the fourteenth century, a flurry of research into this topic began [14]. Many fluids in nature display a nonlinear connection between stress and distortion rate and are referred to as "non-Newtonian fluids" (NNF). Several scientists were interested in exploring the phenomena of movement of these sorts of fluids because of their widespread uses in industries such as unrefined oil extraction from petroleum fuels, food production, paper, and fibre lamination. No single constitutive equation can effectively describe the properties of NNF due to their diversity, different models for such types of fluids have been devised [1]. Casson fluid is one such NNF containing properties such as human blood, jellies, nectar, juice with fibres, etc. This kind of fluid could be useful in medicinal and industrial fields. "Casson fluid is a shear-thinning fluid with infinite viscosity at zero shear rate, yield stress below which no flow occurs, and zero viscosity at the infinite shear rate" [15], [16]. Reference [17] examined the "Natural Convective Non-Newtonian Casson Fluid Flow in a Porous Medium with Slip and Temperature Jump Boundary Conditions" by employing the differential transformation method and Mathematica 9 software. They discovered that as the surge in the value of the magnetic field, the fluid flow decreases. The temperature leap parameter was found to improve the temperature profile. Furthermore, growth in the Casson rheological factor has a considerable impact on fluid flow [17]. Numerous researchers have investigated Casson fluid's movement and heat transfer characteristics from different physical and

Published on May 5, 2022.
A. Prathiba, CVR College of Engineering ,Hyderabad, India.
(corresponding e-mail: alphonsaperli@gmail.com)
A. Venkata Lakshimi, Osmania University, Hyderabad, India.

mathematical perspectives.[9], [15], [18]–[30].

The impact of viscous dissipation is crucial in regular convection in various devices. Viscous dissipation refers to a development in which work performed by a fluid particle is also transformed into heat. It describes the relationship between (K.E) kinetic energy and entropy in a flow and is used to describe dissipation. Another thing is that a fluid flow through porous media has numerous uses in irrigation, farming, civil engineering, and petroleum engineering. Further, "Electromagnetic flow metres, electromagnetic pumps, and hydromagnetic generators" are just a few examples of magnetohydrodynamic (MHD) flows in porous media. In addition to viscous dissipation, when a viscoelastic fluid is forced to flow due to stimulated stress, the energy is accumulated in the solution as strain energy [31]. Darcy's hypothesis, which is valid only for reduced porosity and lowered velocity in most circumstances, is used in most modelling and research of flow through porous mediums. As a result, with "higher flow rates and higher permeability of porous materials, there is a deviation from Darcy's equation, and in this scenario, the inertial impact becomes critical" [2]. Several academics have expressed concern about studying MHD, heat and mass transfer flow in permeable and impermeable mediums [32]–[36]. Gushing through porous media and conventional interactive applications is gaining popularity. Porous materials are used to retain the temperature of the hot body, to line it. The porosity of the porous medium through which MHD flows plays a big role in getting gasoline out of crude oil in the petroleum industry and other fields. MHD tools can be used in a lot of different fields, like material science and medicine [31].

Rotation is critical in managing the heat and mass transfer phenomena in manufacturing and industrial applications. The current work uses the motivations of the previous studies to investigate these transfer characteristics of Casson linear flow across a spinning sheet in the existence of internal friction. The resultant set of linked non-linear governing equations are numerically solved using the Lobatto IIIA method [13], [19], [37]–[41]. The three-stage Lobatto IIIa formula is implemented by BVP4C in MATLAB, a finite difference code. This being a collocation polynomial produces a $4^{th}$ -order accurate continuous solution uniformly in [a, b].

"Mesh selection and error control are based on the continuous solution's residual (http://www.mathworks.com/help/matlab/ref/bvp4c.html#moreabout).Graphs and tables depict the effect of flow controlling parameters on velocity, temperature, and concentration fields, as well as the skin friction coefficient , heat and mass transfer rate".

## II. Modelling The Problem

Contemplate a rotating Casson fluid with a steady, incompressible boundary layer flow induced by the stretching of a heated surface. Because of the *Coriolis force*, the flow is three-dimensional (3-D) [42]. The velocity components in the $(x, y, z)$ direction with axis rotating in z- direction with angular velocity Ω are given by (u, v, w). The surface is considered to be stretching at a rate proportionate to its distance from the origin. The temperature of the stretching surface is held constant at $T_w$, while the temperature of the distant fluid is assumed to be $T_\infty$. Casson fluid has a rheological model that is described as [1]:

$$\tau_{ij} = \begin{cases} 2\left(\mu_B + \dfrac{p_y}{\sqrt{2\pi}}\right)e_{ij}, & \pi > \pi_c \\ 2\left(\mu_B + \dfrac{p_y}{\sqrt{2\pi_c}}\right)e_{ij}, & \pi < \pi_c \end{cases}, \tag{1}$$

Where $\tau_{ij}$ is the *Cauchy stress tensor*, $\pi = (e_{ij})^2$ is the product of deformation rate components with itself, $e_{ij}$ is the $(i,j)^{th}$ deformation rate component, $\pi_c$ is the critical value of a product based on the non-Newtonian model, $\mu_B$ is the non-Newtonian model plastic dynamic viscosity, and $p_y$ is the fluid yield stress [43]. In the present problem, the stress component is $\tau_{xz}$.

Currently $\tau_{xz} = \mu_B\left(1+\dfrac{1}{\beta}\right)\left(\dfrac{\partial w}{\partial x}+\dfrac{\partial u}{\partial z}\right)$ *and* $\dfrac{\partial w}{\partial x}=0$ *where* $\beta = \mu_B\dfrac{\sqrt{2\pi_c}}{p_y}$ is Casson fluid parameter.

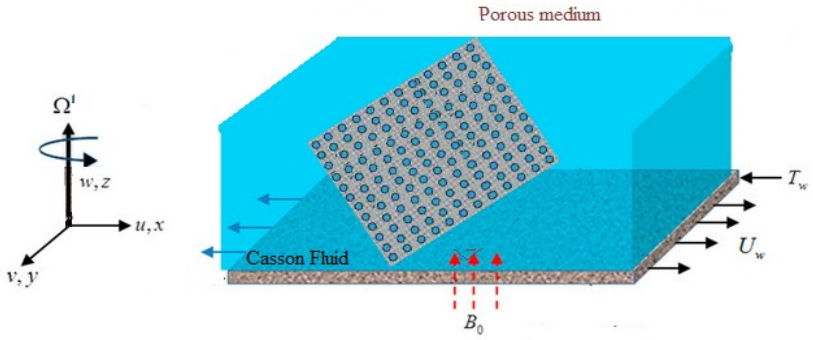


Fig. 1. Sketch of the flow.

Applying the above hypotheses the governing equations for the continuity, momentum and energy, mass diffusion are [2], [43], [44]:

$$\frac{\partial \mathrm{u}}{\partial x}+\frac{\partial \mathrm{v}}{\partial y}+\frac{\partial \mathrm{w}}{\partial z}=0 \tag{2}$$

$$u\frac{\partial u}{\partial x}+v\frac{\partial u}{\partial y}+w\frac{\partial u}{\partial z}-2\Omega' v=\vartheta\left\{1+\frac{1}{\beta}\right\}\frac{\partial^2 u}{\partial z^2}-\frac{\sigma}{\rho}B_0^2 u-\frac{\vartheta u}{k_p^*} \tag{3}$$

$$u\frac{\partial v}{\partial x}+v\frac{\partial v}{\partial y}+w\frac{\partial v}{\partial z}+2\Omega' u=\vartheta\left\{1+\frac{1}{\beta}\right\}\frac{\partial^2 v}{\partial z^2}-\frac{\sigma}{\rho}B_0^2 v-\frac{\vartheta v}{k_p^*} \tag{4}$$

$$u\frac{\partial T}{\partial x}+v\frac{\partial T}{\partial y}+w\frac{\partial T}{\partial z}=\alpha\frac{\partial^2 T}{\partial z^2}+\frac{\mu}{\rho C_p}\left(1+\frac{1}{\beta}\right)\left(\left(\frac{\partial u}{\partial z}\right)^2+\left(\frac{\partial v}{\partial z}\right)^2\right) \tag{5}$$

$$u\frac{\partial C}{\partial x}+v\frac{\partial C}{\partial y}+w\frac{\partial C}{\partial z}=D_M\frac{\partial^2 C}{\partial z^2} \tag{6}$$

The presumed boundary conditions are,

$$\left.\begin{array}{l}\mathrm{u}=U_w\zeta=\hat{a}x\zeta,\mathrm{v}=0,\mathrm{w}=0,\ \mathrm{T}=\mathrm{T}_w,\ \mathrm{C}=\mathrm{C}_w\ \text{ at }\ \mathrm{z}=0\\ \mathrm{u}\longrightarrow 0,\mathrm{v}\longrightarrow 0,\mathrm{w}\longrightarrow 0,\ \mathrm{T}\longrightarrow \mathrm{T}_\infty,\ \mathrm{C}\longrightarrow \mathrm{C}_\infty\ \text{ at }\ \mathrm{z}\longrightarrow\infty\end{array}\right\} \tag{7}$$

where, ($\rho$) "density of the fluid", ($\vartheta$) "coefficient of kinematic viscosity", ($\sigma$) "electrical conductivity", "Casson parameter" ($\beta$), ($k_p^*$) "permeability of the porous medium", (T) fluid temperature, free stream temperature ($\mathrm{T}_\infty$), ($\alpha$) "thermal diffusivity", ($C_p$) "specific heat at constant pressure", and â >0 constant, ($\mathrm{D_M}$) Molecular Diffusivity coefficient, (C) concentration of the species, (ζ) the stretching parameter.

The transformation variables are stated as follows [43], [45]:

$$\eta=\sqrt{\frac{\hat{a}}{\vartheta}}z,\ \mathrm{u}=\hat{a}x\,\mathrm{F}'(\eta),\mathrm{v}=\hat{a}x\,G(\eta),\mathrm{w}=\sqrt{\hat{a}\,\vartheta}\,F(\eta),\theta(\eta)=\frac{T-T_\infty}{T_w-T_\infty},\varphi(\eta)=\frac{C-C_\infty}{C_w-C_\infty} \tag{8}$$

(2) is satisfied by the above transformations and equations (3)-(6) reduce to the following "self-similar ordinary differential equations":

$$\left(1+\frac{1}{\beta}\right)F'''-\left(M^*+k\right)F'-\left(F'\right)^2+F''F+2\omega G=0 \tag{9}$$

$$\left(1+\frac{1}{\beta}\right)G''-\left(M^*+k\right)G-\left(F'G-G'F\right)-2\omega F'=0 \tag{10}$$

$$\theta''+Pr\cdot F\theta'+Pr\cdot Ec\left\{\left(F''\right)^2+\left(G'\right)^2\right\}=0 \tag{11}$$

$$\varphi''+Sc.F\varphi'=0 \tag{12}$$

The comprehensive boundary constrains are attained as:

$$\left.\begin{array}{l} F'(\eta)=\zeta, G(\eta)=0, F(\eta)=0, \theta(\eta)=1, \varphi(\eta)=1 \ \ at\ \eta=0 \\ F'(\eta)\longrightarrow 0, G(\eta)\longrightarrow 0, \theta(\eta)\longrightarrow 0, \varphi(\eta)\longrightarrow 0 \ \ as\ \eta\longrightarrow\infty \end{array}\right\} \tag{13}$$

The parameters in the above equations are given as Magnetic parameter( $M^*=\sigma.B_0^2/\rho$â), Rotation parameter (ω=Ω/â), Porosity parameter ($k\cdot=\vartheta/k_p^*$â), Prandtl Number ($Pr\cdot=\alpha/\vartheta$), Eckert Number ($Ec\cdot=\frac{U_w^2}{Cp(T_w-T_\infty)}$), Schmidt Number ($Sc=\vartheta/D_M$) .

The physical measures of engineering intention i.e., the drag friction coefficient, the reduced Nusselt number, and the Sherwood number are as follows.

$$C_{fx}=\left(1+\frac{1}{\beta\cdot}\right)F''(0), C_{fy}=\left(1+\frac{1}{\beta\cdot}\right)G'(0), Re_x^{-1/2}\,Nu_x=-\theta'(0), Re_x^{-1/2}\,Sh_x=-\varphi'(0),$$

$$Re_x=U_w x/\vartheta\ (local\ Re ynold's\ Number)$$

## III. Solution Methodology

The system of coupled dimensionless (9)-(12) are sensitive to boundary conditions mathematically. Since these equations are highly nonlinear, and solving it analytically is quite challenging. As a result, the bvp4c approach from MATLAB is one of the methods utilised to solve such problems. The numerical solutions are acquired utilising the MATLAB BVP algorithm bvp4c, "a finite difference code that implements the three-stage Lobatto IIIA formula".

In this procedure the (9)-(12) are first metamorphosed into a set of "coupled first-order equations" as follows:

$$f=[F\ F'F''G\ G'\Theta\ \Theta'\Phi\ \Phi']^T$$

$$=\begin{bmatrix} f(1)\\ f(2)\\ f(3)\\ f(4)\\ f(5)\\ f(6)\\ f(7)\\ f(8)\\ f(9) \end{bmatrix} \tag{14}$$

Therefore, the (9) - (12) can be expressed as:

$$\frac{d}{d\eta}\begin{bmatrix} f(1)\\ f(2)\\ f(3)\\ f(4)\\ f(5)\\ f(6)\\ f(7)\\ f(8)\\ f(9) \end{bmatrix}=\begin{bmatrix} f(2)\\ f(3)\\ \dfrac{(M+k)f(2)+f(2)\hat{}2-f(2)f(1)-2\omega f(4)}{\left(1+\frac{1}{\beta}\right)}\\ f(5)\\ \dfrac{(M+k)f(4)+f(2)f(4)-f(5)f(1)+2\omega f(2)}{\left(1+\frac{1}{\beta}\right)}\\ f(7)\\ -Pr\{f(1)f(7)+Ec(f(3)f(3)+f(5)f(5))\}\\ f(9)\\ -Sc\,f(1)f(9) \end{bmatrix}$$

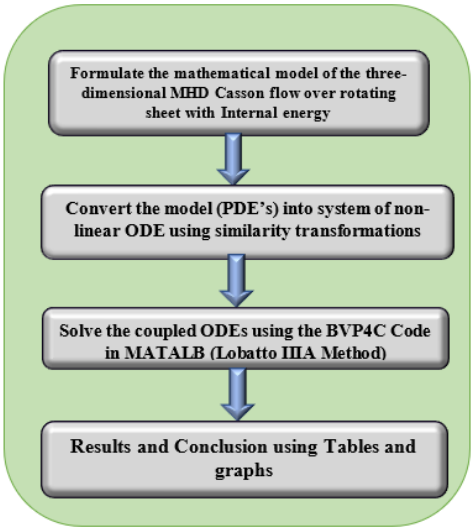


Fig. 2. The graphical scheme of the proposed problem.

This system is known as "boundary value problem (BVP)" and used in MATLAB to find the solution of this system together with the identified boundary conditions using the Lobatto III A RK collocation method (BVP4C) [46]. The procedure will be concluded when the error (tolerance) < $10^{-6}$. Bvp4c has only three arguments when solving the BVP with MATLAB: a 'functionode' for evaluating the ODEs, a 'functionbc' for evaluating the residual in the boundary conditions, and a structure 'solinit' for providing an estimate for a mesh and the solution in it [47]. The ODEs are solved in the same way as the MATLAB IVP solvers. The explanation of this method can found from various research articles [10], [41], [46], [48], [49] .

## IV. Analysis of the Results Obtained

The non-linear ODE of the MHD Casson fluid with viscous dissipation over a rotating sheet with the boundary constraints were solved using the 3-stage Lobatto III A R.K collocation method. The technique was implemented using the symbolic software MATLAB. The boundary conditions were defined at infinity are switched by a sufficiently substantial value $\eta = \eta_{max} = 10$. The accuracy up to six decimal places has been considered for the convergence criteria with a step size of $\Delta\,\eta = 0.001$. The validation of the code was done by comparing the values of physical interest such as drag friction coefficient with the results of [2], [3] and is depicted in Table I.

TABLE I: ASSESSMENT OF CURRENT RESULTS WITH PRIOR COTED RESULTS WHEN $\beta' \to \infty$, Ec=Sc=M*=k=0

| $\omega'$ | Reference [3] | | Reference [3] | | Present Results | |
|---|---|---|---|---|---|---|
| | $-F''(0)$ | $-G'(0)$ | $-F''(0)$ | $-G'(0)$ | $-F''(0)$ | $-G'(0)$ |
| 0 | 1 | 0 | 1 | 0 | 1.000008 | 0 |
| 0.5 | 1.1384 | 0.5128 | 1.13838096 | 0.51276039 | 1.1383812 | 0.51276012 |
| 1 | 1.3250 | 0.8371 | 1.32502883 | 0.83709841 | 1.32502901 | 0.83709845 |
| 2 | 1.6523 | 1.2873 | 1.65235799 | 1.28725883 | 1.65235488 | 1.28725663 |

The choices of the regulating parameters are the "Casson parameter" ($0.5 \le \beta' \le \infty$), rotation parameter ($0.2 \le \omega' \le 3$), the magnetic field parameter ($0 \le M \le 2$), and the "Eckert number" ($0 \le Ec' \le 2$), the "porosity parameter" ($0 < k' < 2$), stretching parameter ($0 < \zeta < 1.5$) and the "Schmidt number" ($0 < Sc < 1$) as demonstrated in the below figures.

Fig. 3 represents the effect of the magnetic parameter (M*) on the "radial velocity gradient (RVG)". One can view from the graph that the RVG weakens for intensification in the magnetic parameter value. Fig. 4 demonstrates the impact of M 'tangential velocity gradient'(TVG). The plotted picture reveals that the spate in values of M* leads to a drop in the TVG. This is for the reason that, like the drag force, a ´transverse magnetic¨ field causes a barrier force (Lorentz force) that retards the movement of the fluid follow. Fig. 5 and 6 exhibits the effect of the porosity parameter on RVG and TVG, where the porous medium permeability opposes particle motion and, as a result, velocity diminishes.

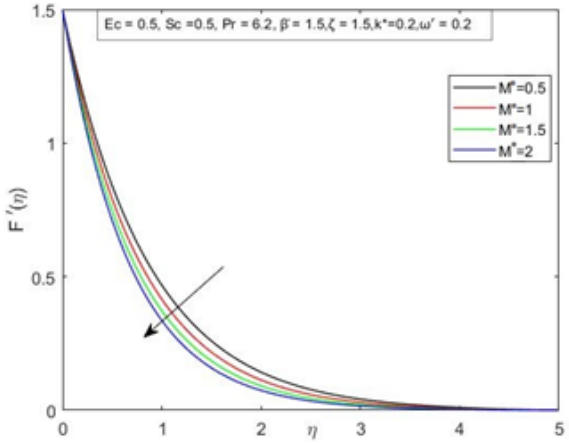


Fig. 3. Impact of magnetic term on RVG.

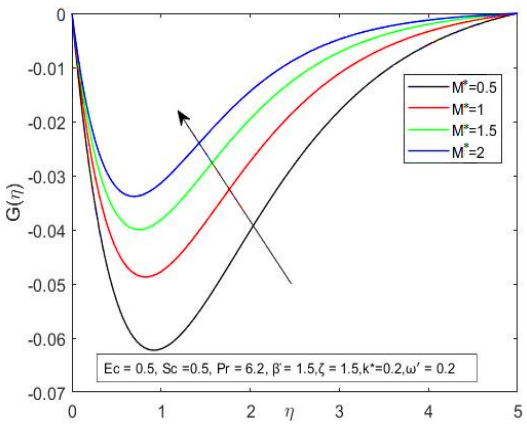


Fig. 4. Behaviour of TVG with magnetic term.

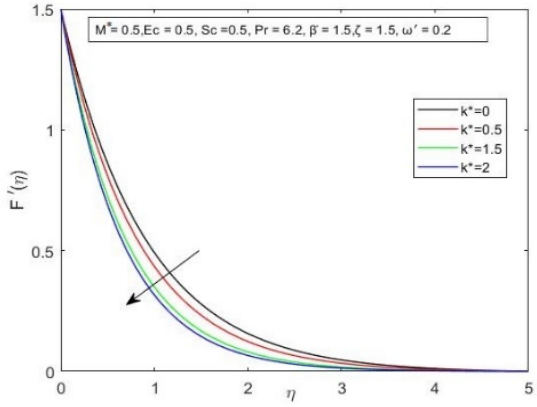


Fig. 5. Effect of porosity on RVG.

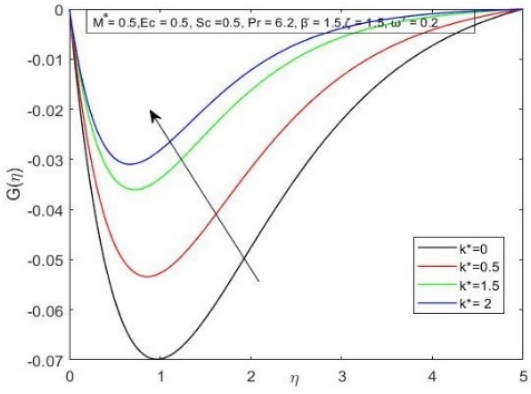


Fig. 6. Effect of porosity on TVG.

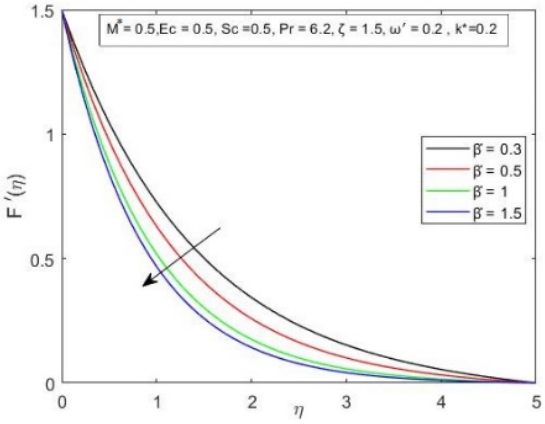


Fig. 7. Effect of Casson parameter on RVG.

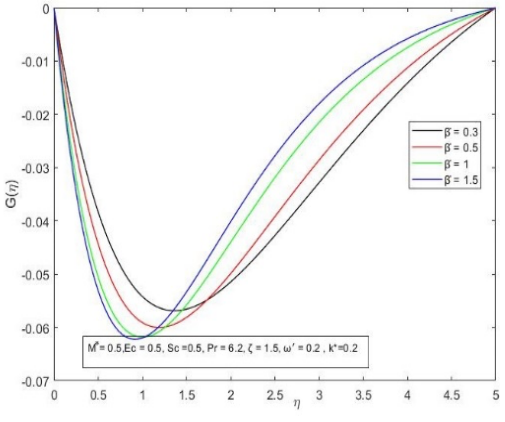


Fig. 8. Effect of Casson parameter on TVG.

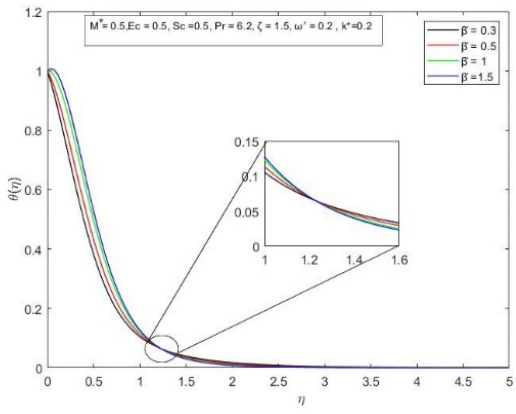


Fig. 9. Performance of Temperature profile with β.

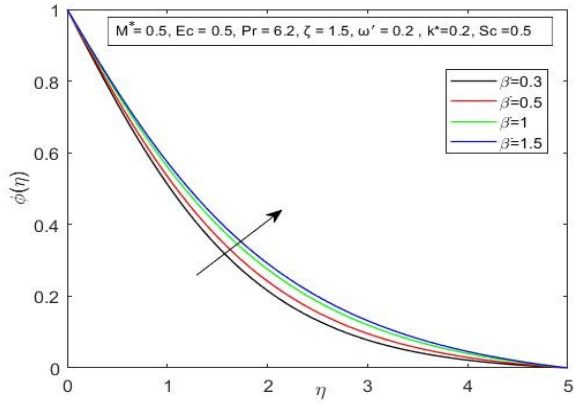


Fig. 10. Performance of Temperature profile with β.

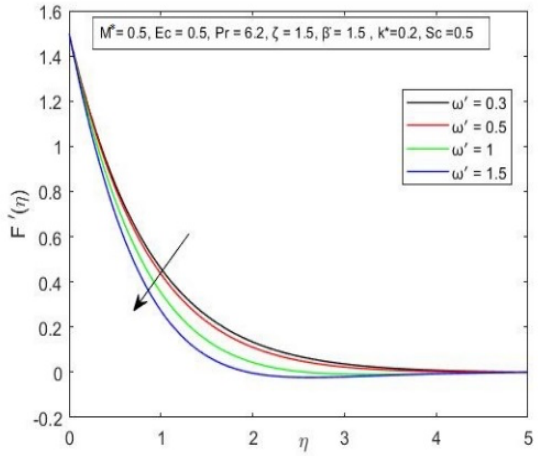


Fig.11. Impact of Rotational parameter on RVG.

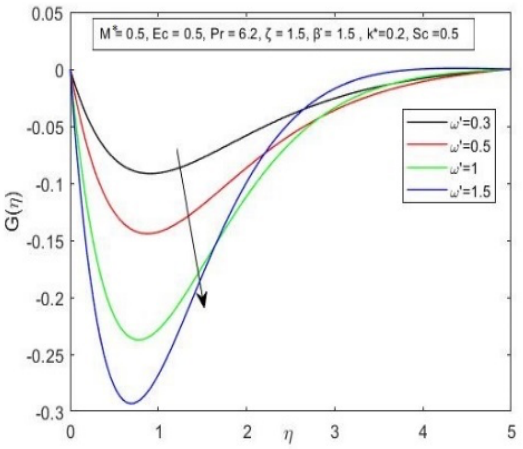


Fig. 12. Impact of Rotational parameter on TVG.

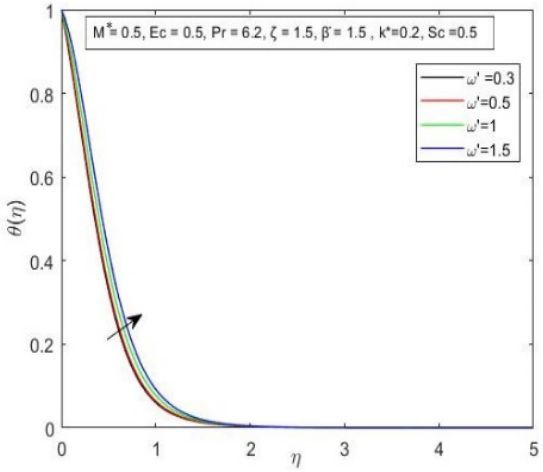


Fig. 13. Influence of ω on temperature profile.

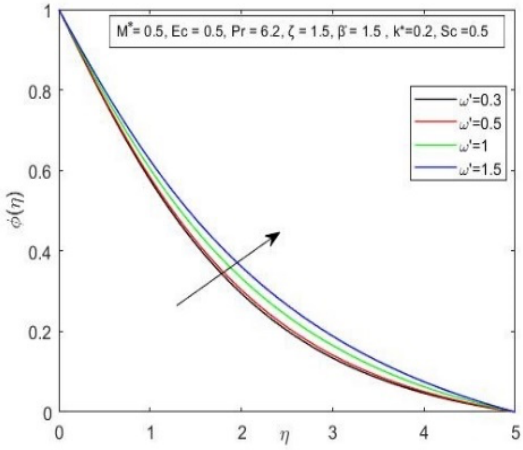


Fig. 14. Influence of ω on the concentration profile.

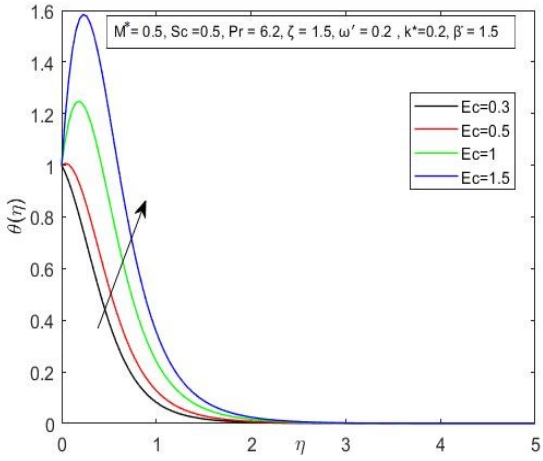


Fig. 15. Effect of Ec on temperature.

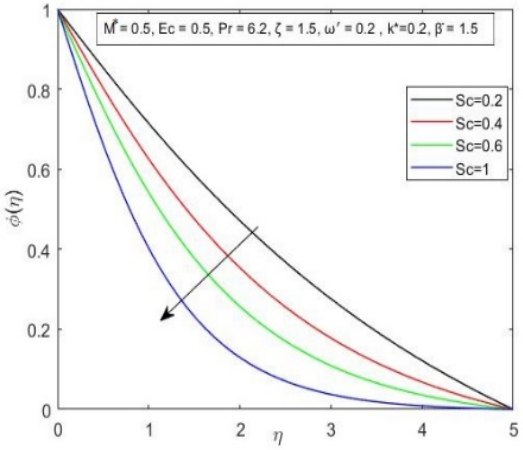


Fig. 16. Effect of Sc on concentration.

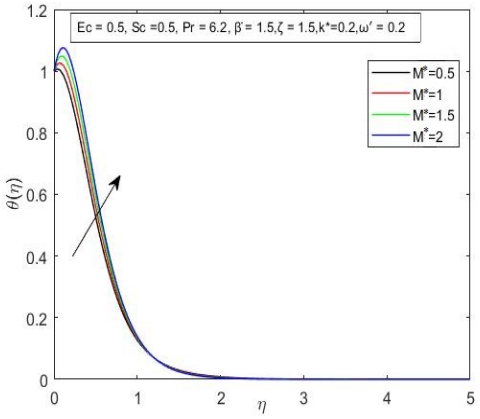


Fig. 17. Effect of Sc on Concentration.

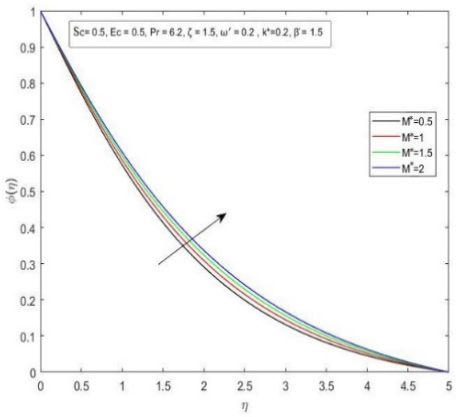


Fig. 18. Effect of magnetic parameter on Concentration

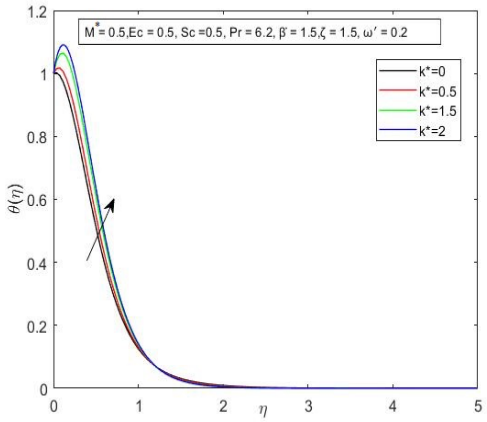


Fig. 19. Effect of porosity on temperature.

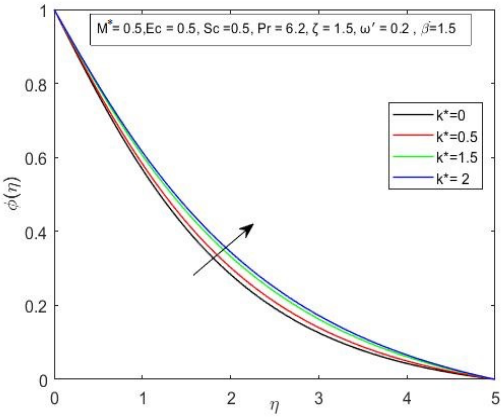


Fig. 20. Effect of porosity on concentration.

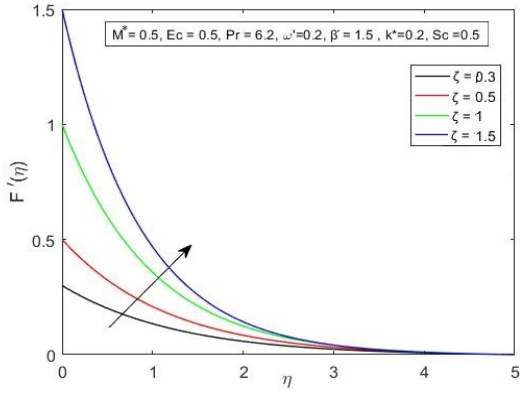


Fig. 21. Performance of RVG with ζ.

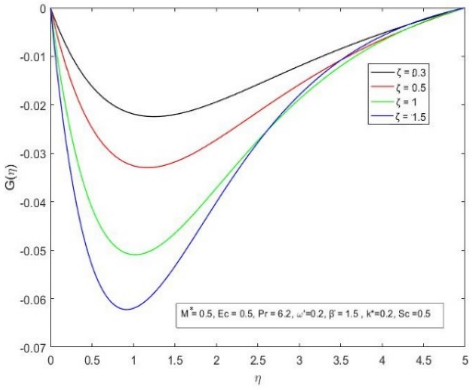


Fig. 22. Performance of TVG with ζ.

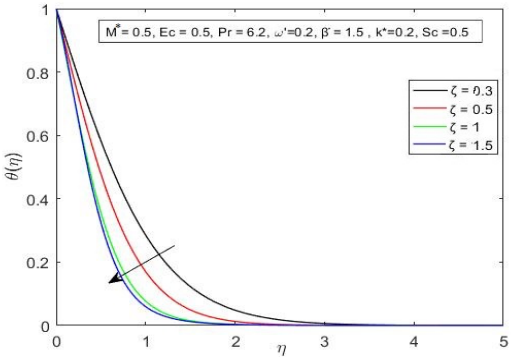


Fig. 23. Behaviour of Temperature with ζ.

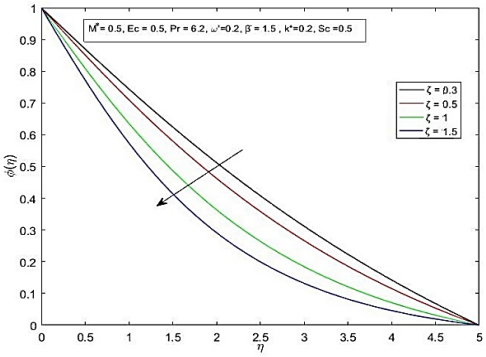


Fig. 24. Behaviour of Concentration with ζ.

Fig. 7 and 8 reveal the influence of the Casson parameter on the RVG and TVG. With an increase in the value of the β, the velocity profiles F' and G decrease. This is because the presence of tensile stress owing

to elasticity causes resistance in the fluid flow, resulting in a decrease in velocities. The thickness of the velocity boundary layer diminishes as β̛ increases. In contrast, as illustrated in Fig. 9 and 10, increasing β̛ leads to a rise in temperature and concentration boundary layers.

Higher rotation parameter values result in lower velocity dispersion. (Fig. 11) In physical terminology, the "rotation parameter (RP) is the ratio of rotation to stretching rates". Elevated values of the RP result in a quicker rotational rate, which the velocity dispersal of RVG and the width of the momentum layer to drop. Fig. 12 depicts the effect of the rotation parameter on the velocity distribution G. In this instance, the velocity distribution is decayed by rising. This is because the rotation parameter is essential for speeding up the flow along the TVG. The velocity distribution oscillates when the rotation parameter is increased. From the Fig. 13 and Fig. 14 we perceive that the rise in the rotation parameter value leads in the increment in the temperature and the concentration boundary layers.

Fig. 15 depicts the effect of the Eckert number on fluid temperature. A higher Eckert number value results in a higher temperature´ gradient. This is due to the number's reliance on K.E, which releases thermal energy into the fluid and hence raises the temperature´.

The impact of the "Schmidt number" on the concentration profile can be visualized in the Fig. 16 shows. For the reason that, as Sc is proportional to the "Brownian diffusion coefficient", bigger 'Schmidt numbers' result in a lower Brownian diffusion coefficient, indicating a lower species concentration. The effects of the magnetic parameter and the porosity parameter on the thermal and concentration boundary layer are depicted in the Figs'. 17, 18, 19 and 20. The result was observed that the increase in these parameter values improved the temperature and concentration boundary layers.

Impact of the (ζ) stretching parameter on the velocity can be noted form the Fig. 21 and 22. The increment in the stretching parameter value leads to the improvement in the RVG and fall in the TVG. This is because when the value of the stretching ratio parameter grows, the rate of stretching increases, implying an increase in velocity field and momentum boundary layer thickness along the y axis. Fig. 23 depicts the result of the stretching ratio parameter on the temperature field. Temperature distribution and the thermal boundary layer are both decreasing functions of ζ. Physically, as the velocity grows, the thermal boundary layer gets weaker along with the drop in the temperature . The similar effect of ζ on the concentration gradient was noted in the Fig. 24. For different value of active parameters in the problem, Table II and III show the values of local drag coefficient in x and y directions, as well as local Nusselt and Sherwood numbers. Local drag coefficient improves in both directions for the Casson parameter, but decreases for the rotation parameter, while the magnetic parameter shows opposite fluctuations. For these settings, the local Nusselt number falls. The rate of heat transmission and rate of change of concentration at the surface reduce when the values of Ec, Sc, k, M change.

TABLE II: THE NUMERICAL VALUES OF THE Cfx, Cfy, Re-1/2xNux, Re-1/2xNux FOR ω̛, Ec

| ω̛ | Ec | Sc | β̛ | k̛ | M* | $\left(1+\frac{1}{\beta}\right)F''(0)$ | $\left(1+\frac{1}{\beta}\right)G'(0)$ | $-\theta(0)$ | $-\varphi(0)$ |
|---|---|---|---|---|---|---|---|---|---|
| 0 | 0.5 | 0.5 | 0.5 | 0.5 | 0.5 | -4.111816 | 0 | 0.41709 | 0.505995 |
| 0.5 | | | | | | -4.21094 | -0.891259 | 0.254713 | 0.49866 |
| 1.5 | | | | | | -4.749054 | -2.314587 | 0.635624 | 0.460403 |
| 2.0 | | | | | | -5.051641 | -2.866752 | -1.141536 | 0.441407 |
| 0.5 | 0.2 | | | | | | | 1.497354 | |
| | 0.4 | | | | | | | 0.75906 | |
| | 0.6 | | | | | | | 0.020768 | |
| | 1 | | | | | | | - 1.455817 | |

TABLE III: THE NUMERICAL VALUES OF THE Cfx, Cfy, Re-1/2xNux, Re-1/2xNux FOR M, k̛, Sc, β̛

| ω̛ | Ec | Sc | β̛ | k̛ | M* | $\left(1+\frac{1}{\beta}\right)F''(0)$ | $\left(1+\frac{1}{\beta}\right)G'(0)$ | $-\theta(0)$ | $-\varphi(0)$ |
|---|---|---|---|---|---|---|---|---|---|
| 0.2 | 0.5 | 0.5 | 0.4 | 0.5 | 0.5 | -4.461336 | -0.391794 | 0.593282 | 0.516321 |
| | | | 0.8 | | | -3.573767 | -0.317512 | -0.050454 | 0.482102 |
| | | | 1.0 | | | -3.369112 | -0.299761 | -0.255903 | 0.472509 |
| | | | 1.5 | | | -3.075365 | -0.274014 | -0.605783 | 0.457436 |
| | | | | 0.4 | | -4.047248 | -0.373375 | 1.161566 | 0.507723 |
| | | | | 0.8 | | -4.363664 | -0.341127 | 1.030058 | 0.496352 |
| | | | | 1 | | -4.514137 | -0.32767 | 0.966215 | 0.491094 |
| | | | | 1.5 | | -4.870999 | -0.299704 | 0.811911 | 0.479036 |
| | | | | | 0.5 | -4.128432 | -0.36454 | 1.128206 | 0.504767 |
| | | | | | 1. | -4.514137 | -0.32767 | 0.966215 | 0.491094 |
| | | | | | 1.5 | -4.870999 | -0.299704 | 0.811911 | 0.479036 |
| | | | | | 2.0 | -5.204276 | -0.277691 | 0.664609 | 0.468317 |
| | | 0.0 | | | | | | | 0.2 |
| | | 0.5 | | | | | | | 0.504767 |
| | | 1.0 | | | | | | | 0.77771 |
| | | 1.5 | | | | | | | 0.99712 |

## V. CONCLUSION

The important outcomes of this study are reviewed below,

1. Radial velocity gradient is affected in the opposite way by rotation and the Casson parameter than Tangential velocity gradient near the extended sheet due to "Coriolis force".
2. The influence of the magnetic field, porosity, and local inertia coefficient on RVG and TVG are identical.
3. The rise in the Eckert number improves the values of the thermal boundary layer and decreases the values of the heat transport coefficient.
4. The increment in the values of Schmidt number leads to the fall in the concentration boundary layer and opposite behaviour is observed by the Sherwood number for those values.

## NOMENCLATURE

| | | | |
|---|---|---|---|
| $u, v, w$ | *x, y, z components of velocity* ($ms^{-1}$) | $T_\infty$ | *Free stream temperature (K)* |
| $C_w$ | *Free stream concentration* | $\rho$ | *Fluid density* ($kgm^{-3}$) |
| $\zeta$ | *Stretching parameter* | $C_\infty$ | *Uniform constant concentration* |
| $T$ | *The temperature of the fluid (K)* | $\Omega'$ | *Angular velocity* |
| $\boldsymbol{D_m}$ | *Mass diffusivity coefficient.* | $B_0$ | *Applied magnetic field* ($Wb\ m^{-2}$) |
| $M^*$ | *Magnetic Parameter* | $\alpha'$ | *Thermal diffusivity* |
| $Cp$ | *Specific heat constant pressure* ($Jkgk^{-1}$) | $\omega'$ | *Angular velocity* |
| $C$ | *The concentration of the species* | $\beta$ | *Casson Parameter* |
| $T_w$ | *Surface temperature (K)* | $Re_x$ | *Local Reynolds number* |
| $v$ | *Kinematic viscosity* ($m^2s^{-1}$) | $Sc$ | *Schmidt number* |
| $Pr$ | *Prandtl number* | $\mu$ | *Dynamic viscosity* ($kgm^{-1}s^{-1}$) |
| | *permeability of porous medium* ($m^2$) | $Ec$ | *Eckert number* |

## ABBREVIATIONS

NNF: Now-Newtonian Fluid
RVG: Radial Veloctiy Gradient
NNM: Non- Newtonian Model
K. E: Kinetic Energy
TVG: Tangential Velocity Gradient

## REFERENCES

[1] Archana M, Gireesha BJ, Prasannakumara BC, Gorla RSR. Influence of nonlinear thermal radiation on rotating flow of Casson nanofluid. *Nonlinear Eng.* 2018; 7(2): 91–101.
[2] Shanker Seth G, Kumar Mandal P. Hydromagnetic rotating flow of Casson fluid in Darcy-Forchheimer porous medium. *MATEC Web Conf.* 2018; 192: 4–7.
[3] Wang CY. Stretching a surface in a rotating fluid. *Z. Angew. Math. Phys.* 1988; 39(2): 177–185.
[4] A. Hussain, Haider Q, Rehman A, Ahmad H, Baili J, Aljahdaly NH, et al. A thermal conductivity model for hybrid heat and mass transfer investigation of single and multi-wall carbon nano-tubes flow induced by a spinning body. *Case Stud. Therm. Eng.* 2021; 28: 101449.
[5] Krishna MV, Ahammad NA, Chamkha AJ. Radiative MHD flow of Casson hybrid nanofluid over an infinite exponentially accelerated vertical porous surface. *Case Stud. Therm. Eng.* 2021; 27: 101229.
[6] Anuar NS, Bachok N, Pop I. Radiative hybrid nanofluid flow past a rotating permeable stretching/shrinking sheet. *Int. J. Numer. Methods Heat Fluid Flow*. 2020; 31(3): 914–932.
[7] Qayyum S, Khan MI, Hayat T, Alsaedi A. Comparative investigation of five nanoparticles in flow of viscous fluid with Joule heating and slip due to rotating disk. *Phys. B Condens. Matter*. 2018; 534: 173–183.
[8] Nadeem S, Saleem S. Theoretical Investigation of MHD Nanofluid Flow Over a Rotating Cone: An Optimal Solutions. *Inf. Sci. Lett.* 2014; 3(2): 55–62.
[9] Salahuddin T, Siddique N, Arshad M, Tlili I. Internal energy change and activation energy effects on Casson fluid. *AIP Adv.* 2020; 10(2).
[10] Shoaib M, Raja MAZ, Sabir MT, Awais M, Islam S, Shah Z, et al. Numerical analysis of 3-D MHD hybrid nanofluid over a rotational disk in presence of thermal radiation with Joule heating and viscous dissipation effects using Lobatto IIIA technique. *Alexandria Eng. J.* 2021; 60(4): 3605–3619.
[11] Ijaz Khan M, Nasir T, Hayat T, Khan NB, Alsaedi A. Binary chemical reaction with activation energy in rotating flow subject to nonlinear heat flux and heat source/sink. *J. Comput. Des. Eng.* 2020; 7(3): 279–286.

[12] Ali B, Naqvi RA, Hussain D, Aldossary OM, Hussain S. Magnetic rotating flow of a hybrid nano-materials ag MoS2 and Go MoS2 in C2H6O2 H2O hybrid base fluid over an extending surface involving activation energy: Fe simulation. *Mathematics*. 2020; 10: 1–22.
[13] Prathiba A, Akavaram VL. Numerical investigation of a convective hybrid nanofluids around a rotating sheet. *Heat Transf*, 2022.
[14] Narender G, Govardhan K, Sarma GS. MHD Casson Nanofluid Past a Stretching Sheet with the Effects of Viscous Dissipation, Chemical Reaction and Heat Source/Sink. *J. Appl. Comput. Mech.* 2021; 7(4): 2040–2048.
[15] Ali A, Farooq H, Abbas Z, Bukhari Z, Fatima A. Impact of Lorentz force on the pulsatile flow of a non-Newtonian Casson fluid in a constricted channel using Darcy's law: a numerical study. *Sci. Rep.* 2020; 10(1): 1–15.
[16] Dash RK, Mehta KN, Jayaraman G. Casson Fluid Flow In A Pipe Filled With A Homogeneous Porous Medium. *Int. J. Engng Sci*. 1996; 34(10): 1145–1156.
[17] Obalalu AM, Ajala OA, Adeosun AT, Wahaab FA, Aliu O, Adebayo LL. Natural Convective Non-Newtonian Casson Fluid Flow in a Porous Medium with Slip and Temperature Jump Boundary Conditions. *Pet. Coal*. 2020; 62(4): 1532–1545.
[18] Sandeep N, Koriko OK, Animasaun IL. Modified kinematic viscosity model for 3D-Casson fluid flow within boundary layer formed on a surface at absolute zero. *J. Mol. Liq*. 2016; 221: 1197–1206.
[19] Umar M, Sabir Z, Imran A, Wahab HA, Shoaib M, Raja MAZ. The 3-D flow of casson nanofluid over a stretched sheet with chemical reactions, velocity slip, thermal radiation, and brownian motion. *Therm. Sci.* 2020; 24(5): 2929–2939.
[20] Mehta RP. Kataria HR. Cross diffusion effects on motion of three dimensional cassion fluid flow past between two horizontal plates in a porous medium. *J. Appl. Sci. Eng.* 2020; 23(2): 319–331.
[21] Gangaiah T, Saidulu N, Venkata Lakshmi A. The influence of thermal radiation on mixed convection MHD flow of a casson nanofluid over an exponentially stretching sheet. *Int. J. Nanosci. Nanotechnol.* 2019; 15(2): 83–98.
[22] Besthapu P, Haq RU, Bandari S, Al-Mdallal OM. Thermal radiation and slip effects on MHD stagnation point flow of non-Newtonian nanofluid over a convective stretching surface. *Neural Comput. Appl.* 2019;31(1): 207–217.
[23] Reza AM, Chahal R, Sharma N. Radiation Effect on MHD Casson Fluid Flow over a Power-Law Stretching. World Academy of Science, Engineering and Technology International Journal of Chemical, Molecular, Nuclear, Materials and Metallurgical Engineering. 2016; 3(5): 46451.
[24] Mangathai P, Reddy BR. Unsteady Mhd Williamson And Casson Nano Fluid Flow In The Presence Of Radiation And Viscous Dissipation. *Turkish Journal of Computer and Mathematics Education (TURCOMAT)*. 2021; 12(13): 1036–1051.
[25] Raju ABMM, Mallikarjuna B. Nonlinear Convective Rotating Casson Fluid Flow Over A Radiated Porous Cone With Rotation And Variable Properties. *Journal of the Korean Physical Society*. 2019; 8(7): 75–92.
[26] Sahoo A, Nandkeolyar R. Entropy generation and dissipative heat transfer analysis of mixed convective hydromagnetic flow of a Casson nanofluid with thermal radiation and Hall current. *Scientific Reports.* 2021; 11(1).
[27] Satya Narayana PV, Tarakaramu N, Sarojamma G, Animasaun IL. Numerical simulation of nonlinear thermal radiation on the 3D flow of a couple stress casson nanofluid due to a stretching sheet. *J. Therm. Sci. Eng. Appl.* 2021; 13(2): 1–10.
[28] Kodi R, Mopuri O. Unsteady MHD oscillatory Casson fluid flow past an inclined vertical porous plate in the presence of chemical reaction with heat absorption and Soret effects. *Heat Transf.* 2021.
[29] Yusof NS, Soid SK, Illias MR, Abd Aziz AS, Mohd Nasir NAA. Radiative Boundary Layer Flow of Casson Fluid Over an Exponentially Permeable Slippery Riga Plate with Viscous Dissipation. *J. Adv. Res. Appl. Sci. Eng. Technol.* 2020; 21(1): 41–51.
[30] Jawad M, Saeed A, Gul T, Bariq A. Mhd darcy-forchheimer flow of casson nanofluid due to a rotating disk with thermal radiation and arrhenius activation energy. *J. Phys. Commun.* 2021; 5(2):. 1–19.
[31] Krishna MV, Chamkha AJ. Hall and ion slip effects on MHD rotating flow of elastico-viscous fluid through porous medium. *Int. Commun. Heat Mass Transf.* 2020; 113: 104494.
[32] Dhanalakshmi M, Jyothi V, Jayarami Reddy K. Soret and Dufour Effects on MHD Convective Flow Past a Vertical Plate Through Porous Medium. *J. Phys. Conf. Ser.* 2019; 1344: 1.
[33] Bhukta D, Dash GC, Mishra SR. Heat and Mass Transfer on MHD Flow of a Viscoelastic Fluid through Porous Media over a Shrinking Sheet. *Int. Sch. Res. Not.* 2014: 1-11.
[34] Mabood F, Shateyi S, Rashidi MM, Momoniat E, Freidoonimehr N. MHD stagnation point flow heat and mass transfer of nanofluids in porous medium with radiation, viscous dissipation and chemical reaction. *Adv. Powder Technol.* 2016; 27(2): 742–749.
[35] Mishra SR, Nayak B, Sharma RP. MHD stagnation-point flow past over a stretching sheet in the presence of non-darcy porous medium and heat source/sink. *Defect Diffus. Forum*. 2017; 374: 92–105.
[36] Sivasankaran S, Niranjan H, Bhuvaneswari M. Chemical reaction, radiation and slip effects on MHD mixed convection stagnation-point flow in a porous medium with convective boundary condition. *Int. J. Numer. Methods Heat Fluid Flow*. 2017; 27(2): 454–470.
[37] Alhamaly AS, Khan M, Shuja SZ, Yilbas BS, Al-Qahtani H. Axisymmetric stagnation point flow on linearly stretching surfaces and heat transfer: Nanofluid with variable physical properties. *Case Stud. Therm. Eng.* 2021; 24.
[38] Lund LA, Omar Z, Raza J, Khan I. Magnetohydrodynamic flow of Cu–Fe3O4/H2O hybrid nanofluid with effect of viscous dissipation: dual similarity solutions. *J. Therm. Anal. Calorim.* 2021; 143(2): 915–927.
[39] Lund LA, Omar Z, Khan I, Sherif ESM. Dual branches of mhd three-dimensional rotating flow of hybrid nanofluid on nonlinear shrinking sheet. *Comput. Mater. Contin.* 2021; 66(1): 127–139.
[40] Shoaib M, Raja MAZ, Sabir MT, Islam S, Shah Z, Kumam P, et al. Numerical investigation for rotating flow of MHD hybrid nanofluid with thermal radiation over a stretching sheet. *Sci. Rep.* 2020; 10(1): 1–15.
[41] Ahmad F, Waqas H, Ayed H, Hussain S, Farooq S, Khan SA, et al. Numerical treatment with Lobatto-IIIa scheme magneto-thermo-natural convection flow of casson nanofluid (MoS2−Cu/SA) configured by a stretching cylinder in porous medium with multiple slips. *Case Stud. Therm. Eng.* 2021; 26: 101132.
[42] Jain S, Choudhary R. Entropy Generation Analysis of Radiative Rotating Casson Fluid Flow Over a Stretching Surface Under Convective Boundary Conditions BT. *Numerical Heat Transfer and Fluid Flow.* 2019: 349–357.
[43] Butt AS, Ali A, Mehmood A. Study of Flow and Heat Transfer on a Stretching Surface in a Rotating Casson Fluid. *Proc. Natl. Acad. Sci. India Sect. A - Phys. Sci.* 2015; 85(3): 421–426.
[44] Senapati M, Swain K, Parida SK. Numerical analysis of three-dimensional MHD flow of Casson nanofluid past an exponentially stretching sheet. *Karbala Int. J. Mod. Sci.* 2020; 6(1): 93–102.
[45] Shah Z, Bonyah E, Islam S, Gul T. Impact of thermal radiation on electrical MHD rotating flow of Carbon nanotubes over a stretching sheet. *AIP Adv.* 2019; 9(1).
[46] Vedavathi N, Dharmaiah G, Venkatadri K, Gaffar SA. Numerical study of radiative non-Darcy nanofluid flow over a stretching sheet with a convective Nield conditions and energy activation. *Nonlinear Eng.* 2021; 10(1): 159–176.
[47] Ibrahim W. Passive control of nanoparticle of micropolar fluid past a stretching sheet with nanoparticles, convective boundary condition and second-order slip. *Proc. Inst. Mech. Eng. Part E J. Process Mech. Eng.* 2016; 231(4): 704–719.

[48] Ouyang C, Akhtar R, Raja MAZ, Touseef Sabir M, Awais M, Shoaib M. Numerical treatment with Lobatto IIIA technique for radiative flow of MHD hybrid nanofluid (Al2O3-Cu/H2O) over a convectively heated stretchable rotating disk with velocity slip effects. *AIP Adv.* 2020; 10(5).
[49] Uddin I, Akhtar R, Zhiyu Z, Islam S, Shoaib M, Raja MAZ. Numerical Treatment for Darcy-Forchheimer Flow of Sisko Nanomaterial with Nonlinear Thermal Radiation by Lobatto IIIA Technique. *Math. Probl. Eng.* 2019; 2019.

**A. Prathiba** is a Sr Assistant Professor at the CVR College of Engineering, Telangana. India. She is also researcher at Department of Mathematics, UCS, Osmania University. Her research interest is in Applied Mathematics, MHD and Fluid Dynamics. https://orcid.org/0000-0003-3044-5935

**A. Venkata Lakshimi** is an Associate Professor at Department of Mathematics, UCS, Osmania University. Her research interest is in Stokes Flows, Special functions, Stability Analysis, Applied Mathematics, MHD and Fluid Dynamics.